Simulation Comparisons and Implementation of Induction Generator Wind Power Systems

T. Manasa[*1], P. Manjusree [2]

[*1] PG [PE&ES] student, Department of EEE, S.R Engineering College, Telangana, India.
[2] Associate professor, Department of EEE, S.R Engineering College, Telangana, India.

ABSTRACT

This paper describes the performance comparison of a wind power systems based on two different induction generators as well as the experimental demonstration of a wind turbine simulator for the maximum power extraction. The two induction machines studied for the comparison are the squirrel-cage induction generator (SCIG) and the doubly fed induction generator (DFIG).

The techniques of direct grid integration, independent power control, and the droop phenomenon of distribution line are studied and compared between the SCIG and DFIG systems. Both systems are modelled in Mat lab/Simulink environment, and the operation is tested for the wind turbine maximum power extraction algorithm results. Based on the simulated wind turbine parameters, a commercial induction motor drive was programmed to emulate the wind turbine and is coupled to the experimental generator systems. The turbine experimental results matched well with the theoretical turbine operation.

1. INTRODUCTION

The Increasing emphasis on renewable wind energy has given rise to augmented attention on more reliable and advantageous electrical generator systems. Induction generator systems have been widely used and studied in wind power system because of their advantages over synchronous generators, such as smaller size, lower cost, and lower requirement of maintenance [1], [2]. The straightforward power conversion technique using squirrel-cage induction generator (SCIG) is widely accepted in fixed-speed applications with less emphasis on the high efficiency and control of power flow. However, such direct connection with grid would allow the speed to vary in a very narrow range and thus limit the wind turbine utilization and power output. Another major problem with SCIG power system is the source of reactive power; that is, an external reactive power compensator is required to hold the distribution line voltage and prevent the whole system from overload.

On the other hand, the doubly fed induction generator (DFIG) with variable-speed ability has higher energy capture efficiency and improved power quality and thus has attracted more attentions. With the advent of power electronic techniques, a back-to-back converter, which consists of two bidirectional converters and a dc link, acts as an optimal operation tracking interface between generator and grid [3]–[5]. Field-oriented control (FOC) is applied to both rotor- and stator-side converters to achieve desirable control on voltage and power [6], [7]. Generally, the FOC has been presented based on DFIG mathematical equations only. However, a three-phase choke is commonly used to couple the stator-side converter into the grid. Therefore, this paper proposes the FOC schemes of stator-side converter involving the choke, and it turns out that both stator- and rotor side converter voltages consist of a current regulation part and a cross-coupling part.

First, this paper presents an experimental setup to emulate the wind turbine operation in torque control mode and thus to obtain a power operation curve for optimal power control. Second, the modelling and simulation of SCIG and DFIG wind systems are studied. Comparison between SCIG without static var compensator (STATCOM) and SCIG with STATCOM as well as DFIG system clearly indicates difference in resulted distribution line voltage.

The paper is organized as follows. The wind turbine is modelled and simulated using the turbine emulator, and an expression of optimal output power versus rotor speed is proposed in Section II. In Section III, the SCIG wind power system is established based on wind turbine system described in Section II. In addition, the DFIG is introduced by mathematical model in Section IV, indicating the relationship of voltage, flux, and torque. At last, steady-state and dynamic experiment/simulation results are presented and discussed in Section 5.

2. WINDTURBINE

Wind energy is extracted through wind turbine blades and then transferred by the gearbox and rotor hub to the mechanical energy in the shaft, which drives the generator to convert the mechanical energy to electrical energy. The turbine model is based on the output power characteristics, expressed as [3], [8]

$$P_m = C_p(\lambda, \beta) \cdot \frac{1}{2}\rho A v_w^3 \quad (1)$$

$$\lambda = \frac{R_{\text{blade}}\omega_r}{v_w} \quad (2)$$

Where P_m is the mechanical output power in watts, which depends on power performance coefficient C_p, air density ρ, turbine swept area A, and wind speed Vw.$(1/2)\cdot\rho A v^3{}_w$ is equal to the kinetic energy contained in the wind at a particular speed Vw. The performance coefficient $C_p(\lambda, \beta)$, which depends on tip speed ratio λ and blade pitch angle β, determines how much of the wind kinetic energy can be captured by the wind turbine system. A nonlinear model describes $C_p(\lambda, \beta)$as [8]

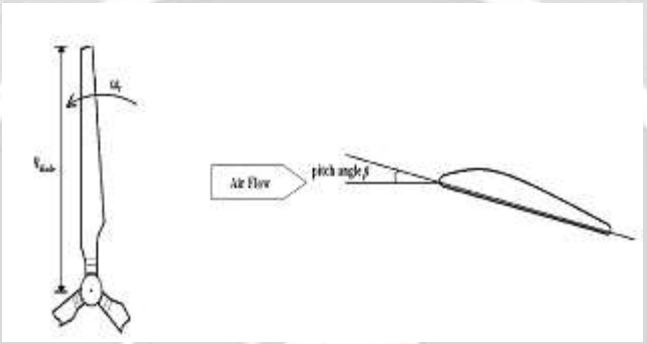

Fig-1: Schematics of turbine blade from different views

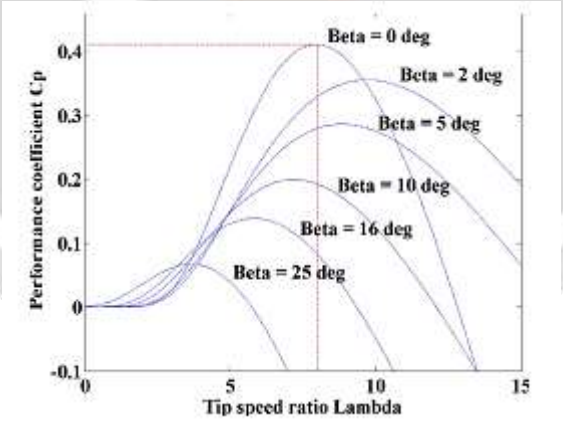

Fig-2: Cp−λ curve for the turbine model

$$C_p(\lambda, \beta) = c_1(c_2 - c_3\beta - c_4\beta^2 - c_5)e^{-c_6} \quad (2)$$

wherec1=0.5, c_2= 116/λi, c_3=0.4, c_4=0,c_5=5, c_6=21/λi, and

$$\frac{1}{\lambda_i} = \frac{1}{\lambda + 0.08\beta} - \frac{0.035}{\beta^3 + 1} \quad (3)$$

Where R_{blade} and ω_r are the blade radius and angular frequency of rotational turbine as depicted in Fig.1. The C_p−λ curve for this particular turbine model at different β is shown in Fig. 2 where it is illustrated that, to achieve maximum Cp, one has β=0◦ and λ=8. The blade with fixed geometry will have fixed C_p−λ

characteristics, as described in (2) and(3). Therefore, to track the optimal output power, the curve of P_m–ω_r is the "map" to follow.

In order to experimentally investigate the operation of wind turbine, a wind turbine emulator system is built to operate in torque control mode, using (1a)

$$T = \frac{P}{\omega_r} = \frac{1}{2}\rho\pi R_{\text{blade}}^3 v_w^2 \frac{C_p}{\lambda} = \frac{1}{2}\rho\pi R_{\text{blade}}^3 v_w^2 C_m \quad (4)$$

Where C_m is the torque performance coefficient. It is dependent on ω_r, v_w, and β. Thus, based on turbine Cp–λ model and by assuming $\beta=0^\circ$,the C_m–λ curve is given in Fig. 3. At any particular v_w, one could obtain different torque and, thus, power output by varying rotor speed. The system configuration is shown in Fig. 4, where the ω_r is fed back to the controller for calculating C_m and, then, torque command.

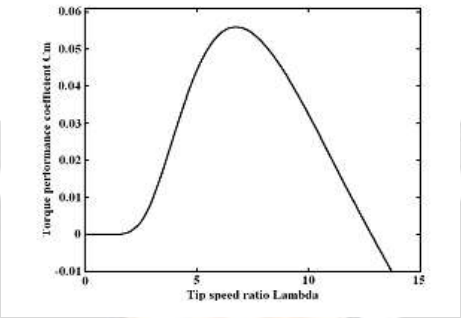

Fig-3: Cm–λcurve for the turbine emulator

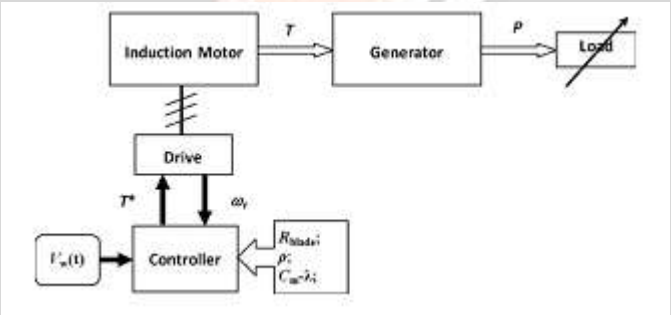

Fig-4: Wind turbine emulator system.

3. SCIG WIND POWER SYSTEM

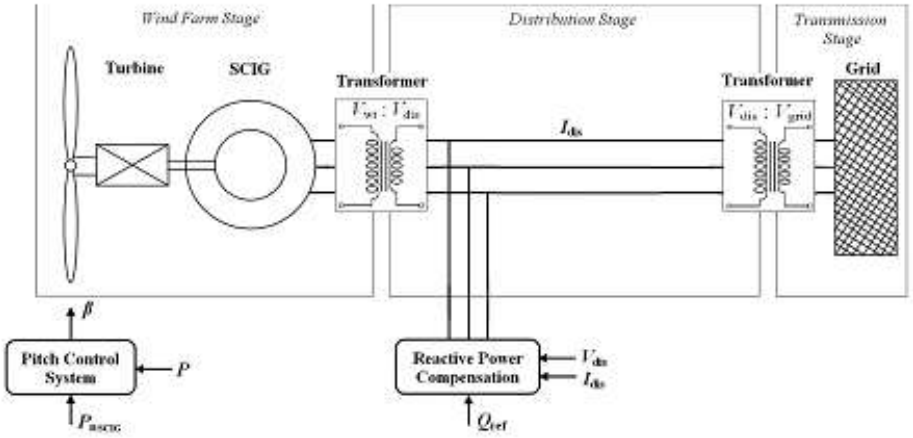

Fig-5: SCIG wind power system topology.

Fig. 5 shows the schematics of the SCIG system including the wind turbine, pitch control, and reactive power compensator. The entire system includes three stages for delivering the energy from wind turbine to the power grid. The first one is wind farm stage which handles with low voltage V_{wt}, the second is distribution stage which has medium voltage V_d is, and the third is grid transmission stage which has high voltage V_{grid}. The three-

phase transformers take care of the interface between stages [9]. As mentioned, nominal power P_{nSCIG} is considered as active power reference to regulate the pitch angle while V_d is and Id is denote the distribution line-to-line voltage and phase current, and they are monitored to favour the reactive power compensation for distribution line. This fairly straightforward technique was first used since it is simple and has rugged construction, reliable operation, and low cost. However, the fixed-speed essential and potential voltage instability problems severely limit the operations of wind turbine [1], [3].

Since SCIG is of fixed-speed generator, for a particular wind speed, the output active power is fixed as well. Thus, with the increase of wind speed, so does the output power until the nominal power is reached. The wind speed at this moment is called nominal wind speed. Beyond this speed, the pitch angle system will prevent the output power from exceeding the nominal value. That is, when the wind speed is below nominal value, the power capture can vary with the change of wind speed; and when the wind speed is above nominal value, the pitch angle control system will limit the generated power by changing the pitch angle. In such way, the output power will be stabilized at nominal value where the wind speed is always above nominal speed. The pitch angle is determined by an open loop control of regulated output active power and by that shown in Fig. 6.

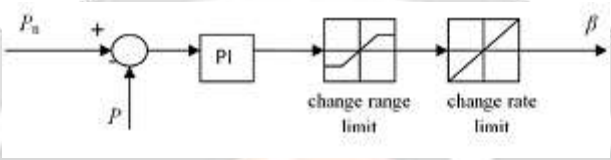

Fig-6: Pitch angle control.

Due to the huge size of blade and, thus, inertia, pitch angle has to change in a slow rate and a reasonable range. It is also worthy to notice that, without reactive power source, in Section V, the SCIG system tends to lead to a voltage droop in distribution line which will cause overload problem. In the simulation section, the comparison between SCIG systemwith and without STATCOM is conducted.

4. DFIG WIND POWER SYSTEM

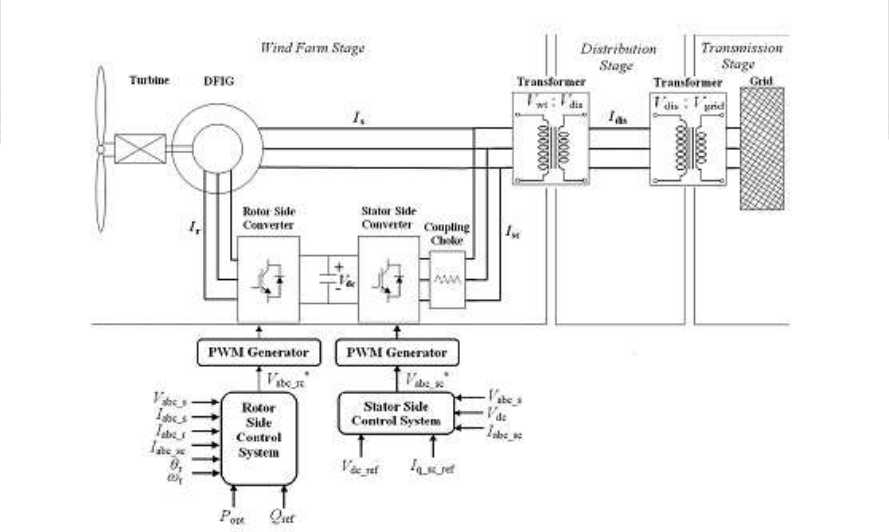

Fig-7: Wind turbine–doubly fed induction generator system configuration.

Traditionally, the dynamic slip control is employed to fulfil the variable-speed operation in wind turbine system, in which the rotor windings are connected to variable resistor and control the slip by the varied resistance [3], [10]. This type of system can achieve limited variations of generator speed, but external reactive power source is still necessary. Consequently, to completely remove the reactive power compensation and to control both active and reactive power independently, DFIG wind power system is one of most popular methods in wind energy applications [1], [3], [7]. This paper reproduces DFIG model first of all and then concentrates on the controlling schemes of power converters, in which the active and reactive power are controlled independently. In particular, the stator-side converter control involving an RL series choke is proposed. Both controlling of rotor- and stator side converter voltages end up with a current regulation part and a cross-coupling part. The wind turbine driving DFIG wind power system consists of a wound-rotor induction generator and an

ac/dc/ac insulated gate bipolar transistor (IGBT)-based pulse width-modulated (PWM) converter (back-to-back converter with capacitor dc link), as shown in Fig. 7. In this configuration, the back-to-back converter consists of two parts: the stator-/grid-side converter and the rotor-side converter. Both are voltage source converters using IGBTs, while a capacitor between two converters acts as a dc voltage source. The generator stator windings are connected directly to grid (with fixed voltage and frequency of grid) while the rotor winding is fed by rotor-side converter through slip rings and brushes, at variable frequency.

The control system is divided into two parts—stator-side converter control system and rotor-side converter control system. An equivalent circuit of DFIG is depicted in Fig. 8, and the relation equations for voltage V, current I, flux Ψ, and torque Te involve [4], [11], [12] are:

$$V_{ds} = R_s I_{ds} - \omega_s \Psi_{qs} + \frac{d\Psi_{ds}}{dt}$$
$$V_{qs} = R_s I_{qs} + \omega_s \Psi_{ds} + \frac{d\Psi_{qs}}{dt} \quad (5)$$

$$V_{dr} = R_r I_{dr} - s\omega_s \Psi_{qr} + \frac{d\Psi_{dr}}{dt}$$
$$V_{qr} = R_r I_{qr} + s\omega_s \Psi_{dr} + \frac{d\Psi_{qr}}{dt} \quad (6)$$

$$\Psi_{ds} = L_s I_{ds} + L_m I_{dr}$$
$$\Psi_{qs} = L_s I_{qs} + L_m I_{qr} \quad (7)$$

$$\Psi_{dr} = L_r I_{dr} + L_m I_{ds}$$
$$\Psi_{qr} = L_r I_{qr} + L_m I_{qs} \quad (8)$$

$$T_e = \frac{3}{2} n_p (\Psi_{ds} I_{qs} - \Psi_{qs} I_{ds}) \quad (9)$$

Where $L_s = L_{ls} + L_m$; $Lr = L_{lr} + L_m$; $s\omega_s = \omega_s - \omega_r$ represents the difference between synchronous speed and rotor speed; subscripts r, s, d, and q denote the rotor, stator, d-axis, and q-axis components, respectively; T_e is electromagnetic torque; and L_m, n_p, and Jare generator mutual inductance, the number of pole pairs, and the inertia coefficient, respectively.

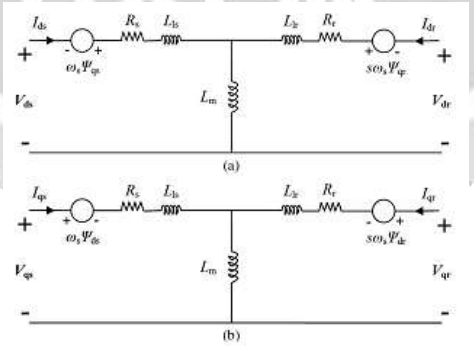

Fig- 8: Equivalent circuit of DFIG. (a)d-axis model. (b)q-axis model

A. Rotor-Side Converter Control

If the derivative parts in (5) are neglected, one can obtain stator flux as

$$\Psi_{ds} = (V_{qs} - R_s I_{qs})/\omega_s$$
$$\Psi_{qs} = (V_{ds} - R_s I_{ds})/(-\omega_s)$$
$$\Psi_s = \sqrt{\Psi_{ds}^2 + \Psi_{qs}^2}. \quad (10)$$

Because of being directly connected to the grid, the stator voltage shares constant magnitude and frequency of the grid. One could make the d-axis align with stator voltage vector; it is true that $V_s=V_{ds}$ and $V_{qs}=0$, thus $\Psi_s=\Psi_{qs}$ and $\Psi_{ds}=0$, which is of stator-voltage-oriented vector control scheme, as

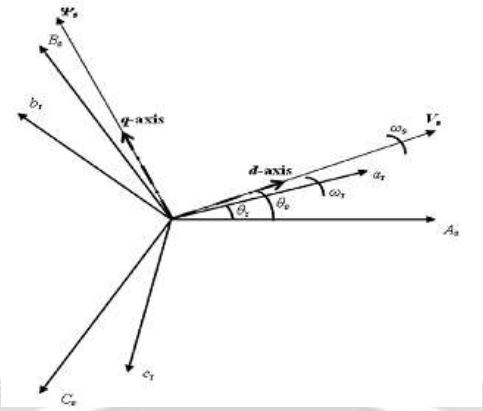

Fig-9: Stator voltage FOC reference frame.

depicted in Fig. 9. According to (7)–(9), the rotor-side converter reference current is derived as

$$I_{dr\_ref} = -\frac{2L_s T_e}{3n_p L_m \Psi_s} \tag{11}$$

Where

$$P_{e\_ref} = P_{opt} - P_{loss} = T_e \omega_r$$
$$P_{loss} = R_s I_s^2 + R_r I_r^2 + R_c I_{sc}^2 + F\omega_r^2 \tag{12}$$

Where I_{sc}, R_c, and Fare stator-side converter current, choke resistance, and friction factor, respectively. P_{opt}, P_{e_ref}, and Ploss are desired optimal output active power, reference active power, and system power loss. Combining (10)–(12), the active power is used as command inputs to determine current reference I_{dr_ref}. Meanwhile, the output reactive power is the stator reactive output power since the stator-side converter's reactive power is set to be zero. Then, one has

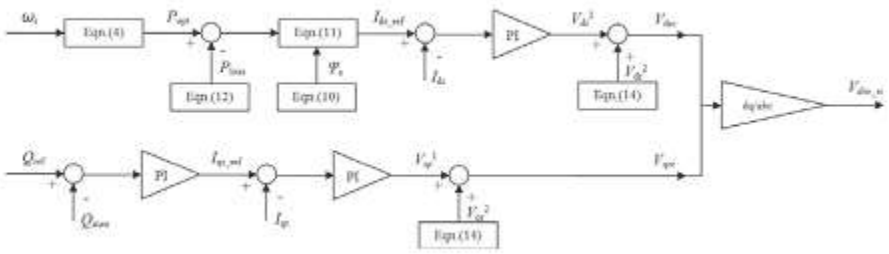

Fig-10: Rotor-side converter control scheme

$$Q_o = Q_s + Q_{sc} = Q_s = \mathrm{Im}\left[(V_{ds} + jV_{qs})(I_{ds} + jI_{qs})^*\right] = V_{ds}I_{qs} - V_{qs}\frac{1}{L_m}(\Psi_s - L_m I_{ds}) \tag{13}$$

Thus, the regulation of reactive power can lead toI_{qr_ref}, and then, the rotor-side converter voltage signals V_{1dr}andV_{1qr} are derived by the regulation of currents. In addition, the feed forward coupling partsV_{2dr} and$V_{2qr}$are derived based on (6) and(8), as

$$V_{dr}^2 = R_r I_{dr} - s\omega_s(L_r I_{qr} + L_m I_{qs})$$
$$V_{qr}^2 = R_r I_{qr} + s\omega_s(L_r I_{dr} + L_m I_{ds}) \tag{14}$$

where the superscripts 1 and 2 denote the current regulation part and cross-coupling part, respectively. At last, rotor-side converter voltage signals in dq-axes are expressed as

$$V_{drc} = V_{dr} = V_{dr}^1 + V_{dr}^2$$
$$V_{qrc} = V_{qr} = V_{qr}^1 + V_{qr}^2 \tag{15}$$

where subscript rc denotes the rotor-side converter. After the conversion of dq−abc, the rotor-side converter voltage V_{abc_rc} can be obtained. Fig. 10 exhibits the control scheme for the aforementioned procedure.

B. Stator-Side Converter Control

Concerning the use of three-phase series RL choke between stator- and stator-side converter, a cross-coupling model is required to derive the voltage signal of stator-side converter, as described in Fig. 11

$$V_{dsc} = V_{ds} - V_{dch}$$
$$V_{qsc} = V_{qs} - V_{qch} \quad (16)$$

where the subscri ptssc and chde note the variables of stator side converter and choke. The coupling part of voltage signals V^2_{dch} and V^2_{qch} is expressed as

$$V^2_{dch} = R_c I_{dsc} - \omega_s L_c I_{qsc} \;, V^2_{qch} = R_c I_{qsc} + \omega_s L_c I_{dsc} \quad (17)$$

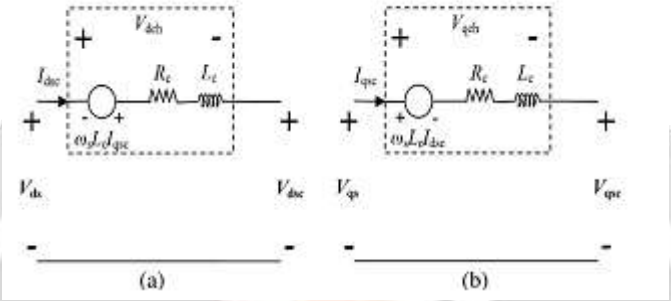

Fig-11: Equivalent circuit of stator-side-converter choke. (a)d-axis model. (b)q-axis model.

Moreover, V^1_{dch} and V^1_{qch} are determined by the regulation of currents I_{ds} c and I_{qsc} in which the current reference Iqsc_ref is given directly while I_{dsc_ref} is determined by the regulation of dc-link voltage V_{dc}. Thus, above all, the stator-side converter voltage signals V_{dsc} and V_{qsc} are obtained as follows and depicted in Fig. 12:

$$V_{dsc} = V_{ds} - V^1_{dch} - V^2_{dch}$$
$$V_{qsc} = V_{qs} - V^1_{qch} - V^2_{qch} \quad (18)$$

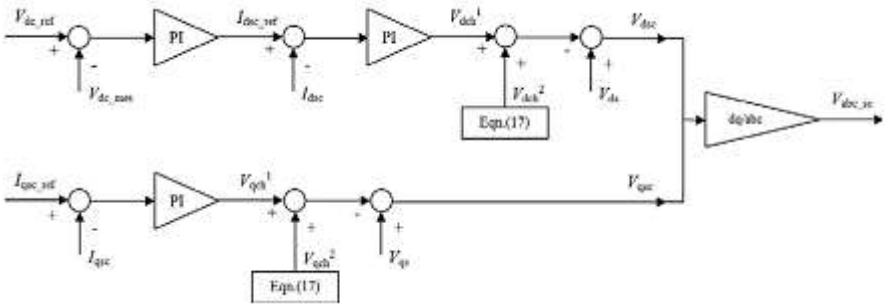

Fig-12: Stator-side converter control scheme.

5. SIMULATION ANALYSIS AND RESULTS

A. SCIG

A traditional SCIG wind power system is developed in Matlab/Simulink, and the related system data used are given in Table II. In order to investigate the system performances, a ramp wind speed v_w is assumed that varies from t=10stot=16s and, then, it remains constant to the end of simulation t=40s. Fig. 13(a)–(e) shows the dynamic variations and steady states of pitch angle β, generator speed ω_r, produced active power P, and consumed reactive power Q. First, he fluctuation in the results during t=0to 2.5 s is due to the initial conditions. In the simulation, the initial speed of generator is set at slip s=−0.01p.u. with respect to synchronous speed and, then, response to the wind speed input disturbance. Other initial values for power and voltages are zero. Since it is lower than nominal value of 0.855 MW, pitch angle control is not working. After t=10s, with the increase of v_w, so do the ω_r and P until t=13s when v_w exceeds the nominal value (11 m/s).

TABLE II
SCIG-BASED WIND POWER SYSTEM PARAMETERS

Parameter	Value
Nominal Wind Speed v_w	11 m/s
Nominal Active Power P_{nSCIG}	0.855 MW
Grid Voltage V_{grid}	120 kV
Grid Frequency f_{grid}	60 Hz
Distribution Line Voltage V_{dis}	12.5 kV
Wind Turbine Bus Voltage V_{wt}	575 V
Stator Resistance R_s	0.0048 p.u.
Stator Leakage Inductance L_s	0.1248 p.u.
Rotor Resistance R_r	0.0044 p.u.
Rotor Leakage Inductance L_r	0.1791 p.u.
Mutual Inductance L_m	6.77 p.u.
STACOM Constant Voltage V_{dc}	4 kV
STACOM Equivalent Capacitance C	625 μF

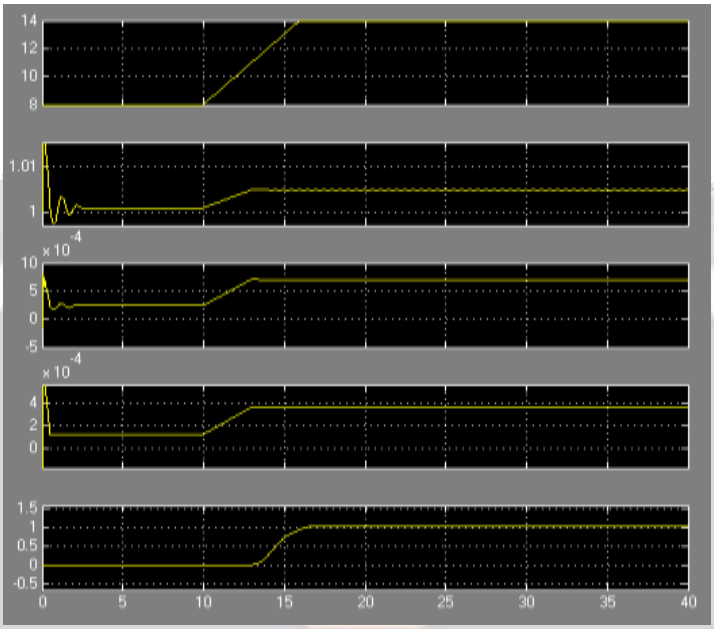

Fig-13: Simulation results for SCIG system: (a) Wind speed v_w; (b) generator speed ω_r; (c) active power P; (d) reactive power Q; (e) pitch angle β.

This is because the pitch control is triggered to limit the increase of output power P and Q as shown in Fig. 13(b)–(d). In this way, the pitch control effectively limits the output P around the nominal value of 0.855 MW and settles a new pitch angle at roughly t=17s.

It is noted that the rotor speed can only vary in very small scope around 1 p.u. (fixed-speed system) and, thus, impossible to achieve optimal active power output. Thus, the active power outputs at v_w=8m/s and≥11 m/s in SCIG are 0.29 and 0.855 MW which are lower than those in later DFIG system. Also, without independent control ability, SCIG system consumes reactive power of 0.41 Mvar in the steady state, which will lead to line voltage droop. To provide necessary reactive power, a STATCOM is added on the distribution line to investigate the improvement.

B. DFIG

By using the proposed optimal power curve as well as the system parameters listed in Table III, the DFIG wind power system is simulated. The DFIG system allows the optimal (maximum) output power operation in the absence of reactive power source. Also, the independent control of active and reactive power is achieved. In the Matlab/Simulink model, the converter switch frequency is set to be 27 times the grid frequency f. To achieve acceptable accuracy, the power circuit and the control circuit models are discretized at different time steps. It is worthy to note that the nominal apparent power and nominal active power are considered as nominal electrical power and nominal mechanical power in this wind power system [3], [13]. Simulation and control system parameters are listed in Table IV and are preloaded into workspace before running the simulation and easy to be modified in m-file.

TABLE III
DFIG-BASED WIND POWER SYSTEM PARAMETERS

Parameter	Value
Nominal Wind Speed v_w	11 m/s
Nominal Apparent Power S_e	1.67 MVA
Nominal Active Power P_{nDFIG}	1.5 MW
Power Factor pf	0.9
Grid Voltage V_{grid}	120 kV
Grid Frequency f	60 Hz
Distribution Line Voltage V_{dis}	12.5 kV
Wind Turbine Bus Voltage V_{wt}	575 V
Generator Number of Pole Pairs n_p	3
Stator Resistance R_s	0.0071 p.u.
Stator Leakage Inductance L_s	0.171 p.u.
Referred Rotor Resistance R_r	0.005 p.u.
Referred Rotor Leakage Inductance L_r	0.156 p.u.
Stator-to-Grid Coupling Resistance R_c	0.003 p.u.
Stator-to-Grid Coupling Inductance L_c	0.3 p.u.
Mutual Inductance L_m	2.9 p.u.
Nominal DC-link Voltage V_{dc}	1.2 kV
DC-link Capacitance C	10 mF
Maximum C Converter Current I_{conv_max}	0.5 p.u.
System Inertia Coefficient H	5 second
Generator Friction Damping F	0.01 p.u.

TABLE IV
SIMULATION AND CONTROL PARAMETERS

Parameter	Value
Power System Sampling Period T_{s_Power}	5e-6 sec
Control System Sampling Period $T_{s\_Control}$	1e-4 sec
Switch Frequency f_{sw}	1620 Hz
Transmission Distance D_{tran}	30 km
Reactive Power Regulator Coefficients K_p; K_i	0.05; 5
DC-link Voltage Regulator Coefficients K_p; K_i	0.002; 0.1
Rotor-side Current Regulator Coefficients K_p; K_i	0.3; 8
Stator-side Current Regulator Coefficients K_p; K_i	2.5; 500

First of all, the steady-state results of the system are shown in Fig. 14(a)–(d), where four wind speed cases Vw= 7,9,10, and12m/s to verify the optimal power output tracking are presented. All of them kept the bus voltage at 1200 Vdc, indicating the well operation of stator-side converter, while the reactive power is set to be zero as the input command. In order to track the optimal active power output, optimal rotor speeds are implemented accordingly. Similarly, the optimal trackings of output power and rotor speed are exhibited in other wind speed cases as well. Therefore, it can be concluded that the system works well to follow the optimal power control at steady-state operation. It is noticed that P and Q are vanished during the first cycle (1/60 s) in displayed result because of the calculation time cost.

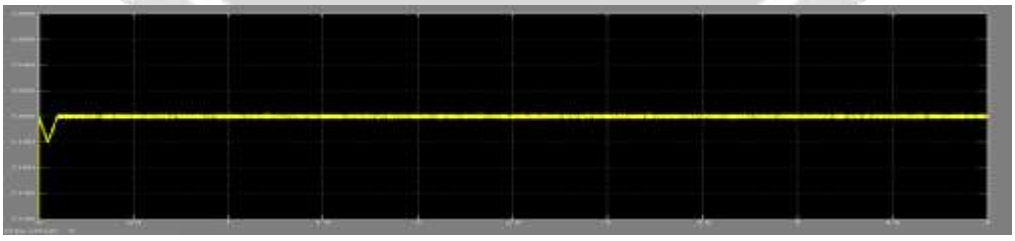

(a)

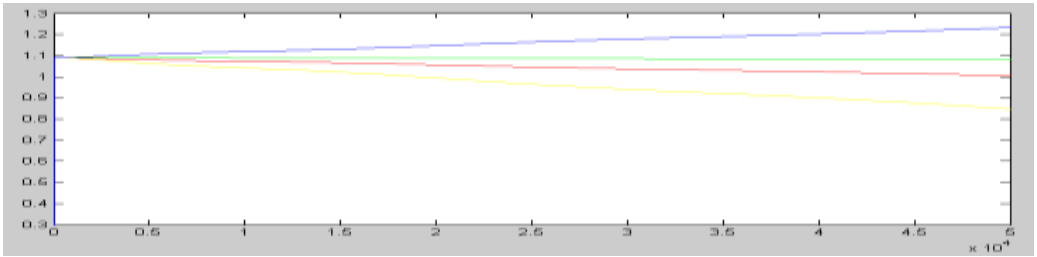

(b)

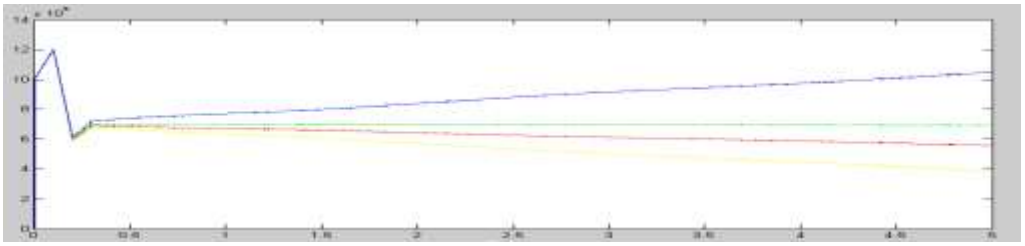

(c)

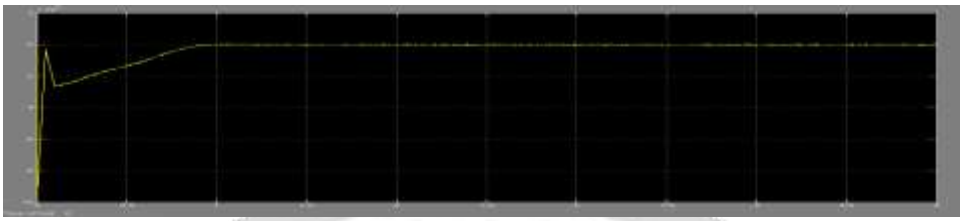

(d)

Fig-14: System responses to different constant wind speeds. (a) DC-link voltage V_{dc}. (b) Rotor speed ωr. (c) Active power P. (d) Reactive power Q

Second, the system dynamic response to varied wind speeds is investigated. Due to the large H of the system, dynamic variation can last and be observed in a long time period before converging to the steady-state values. To shorten such period, H=0.1s is used in this part of simulation. With stable steady-state initial values, three regular types of wind speeds are examined for dynamic responses, including step, ramp, and gusty winds. The varied winds and corresponding results for Vdc, ωr, P, and Q are shown in Figs. 14 and 15, where the system can always reach a new optimal steady state after a few seconds. In the aforementioned results, the reduced inertia constants can only decrease the converging time, making the system reach a new steady state quicker, and it has no effects on steady-state values.

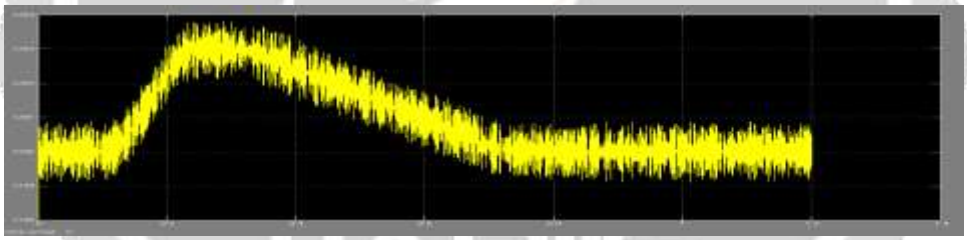

(a)

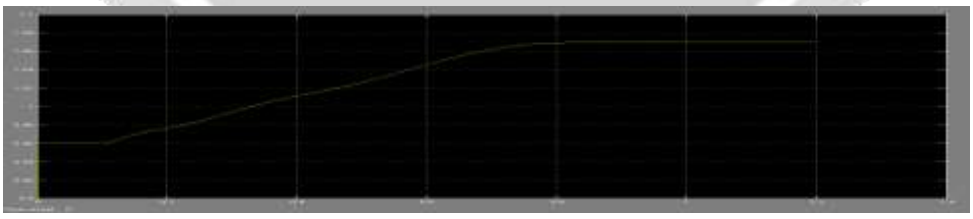

(b)

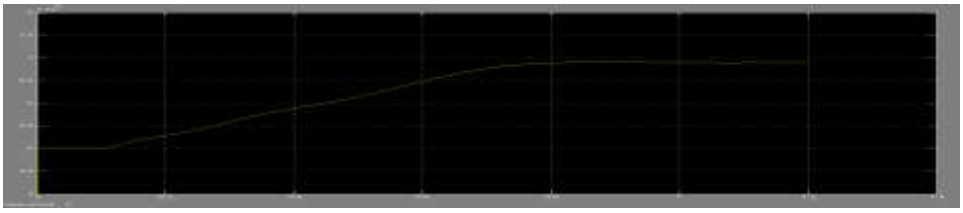

(c)

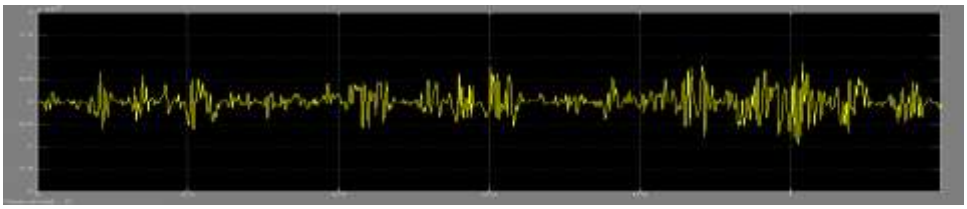

(d)

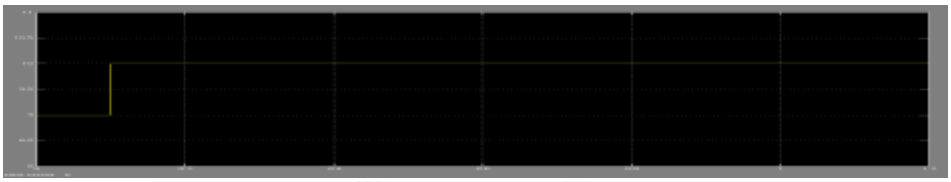

(e)

Fig-15:. Wind step response. (a) DC-link voltage Vdc. (b) Rotor speed ωr. (c) Active power P. (d) Reactive power Q. (e) Wind speed v_w

At last, the system dynamic response to a grid disturbance is investigated. At Vw=9m/s, a remote voltage droop in grid is programmed from t=0.09to 0.29 s. The dynamic responses represented in Fig. 15. During this process, since the wind speed remains the same, control system effectively makes the system recovers in approximate 0.1 s.

C. Comparison between Two Systems

A summary of SCIG and DFIG systems is presented in Table V based on research of this paper.

TABLE V
SUMMARY OF SCIG AND DFIG WIND POWER SYSTEMS

	SCIG	DFIG
Speed Operation	fixed or limited variable	variable
Line Voltage	drop by 0.05 p.u.	stable constant
Control Scheme	pitch control	FOC
Active Power	varies with v_w but not optimally	varies with v_w optimally
Reactive Power	uncontrollable; need compensation	controllable
Power Rating	< 1MW	> 1MW
Cost and Complexity	low and simple	high

The comparison shows the superiority of DFIG system over SCIG system in terms of efficiency, controllability, and high-power applications. Also, the higher cost of slip rings and power electronics can be compensated by more power output.

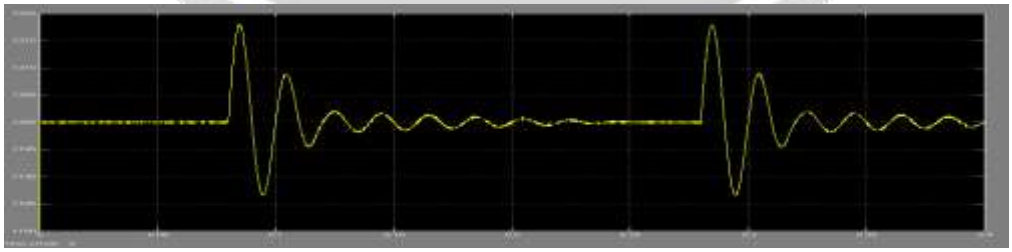

(a)

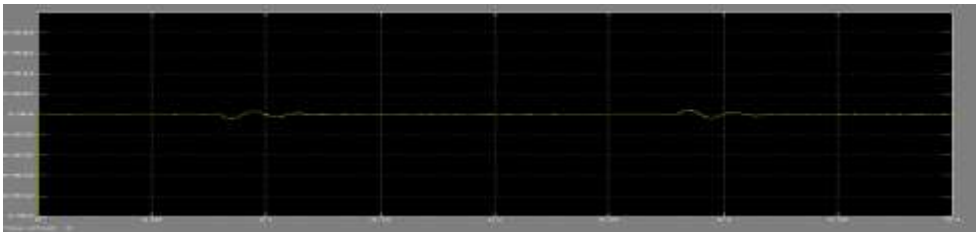

(b)

(c)

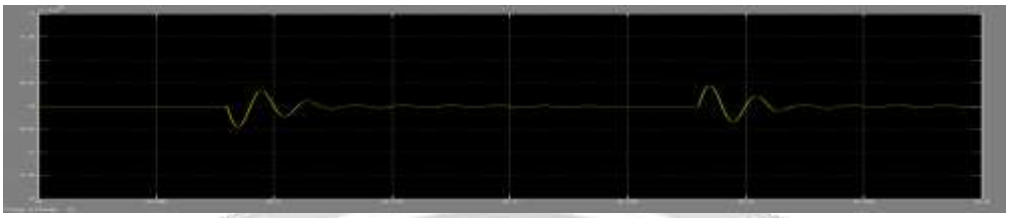

(d)

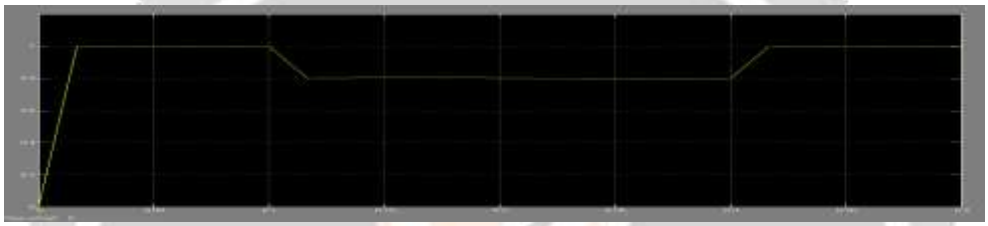

(e)

Fig-16: Dynamic responses to grid voltage droop. (a) DC-link voltage V_{dc}. (b) Rotor speedω_r. (c) Active power P. (d) Reactive power Q. (e) Grid voltage V_{grid}.

6. CONCLUSION

This paper has presented the comparison of the wind turbine systems using SCIG and DFIG generator systems. With the experimentally investigated wind turbine model, a SCIG and a DFIG wind power systems are modelled and simulated in Matlab/Simulink. An optimal active-power-versus-rotor-speed relationship has been proposed for turbine model first, and it functions as a lookup table for tracking the maximum output active power. The SCIG system presents the need of external reactive power source to support grid voltage, and it can keep the output power at the nominal level by pitch control but cannot accordingly change the rotor speed to achieve maximum wind power capture at different wind speeds.

In contrast, the DFIG system does not need reactive power compensator to hold distribution line voltage and achieves optimal active power controlling. Both voltage control schemes for two converters consist of a current regulation part and a cross-coupling part. The turbine emulator system performs well and follows the theoretical and simulated maximum power extraction points in different operating conditions.

REFERENCES

[1] M. Orabi, T. Ahmed, and M. Nakaoka, "Efficient performances of induction generator for wind energy utilization," inProc. 30th Annu. Conf. IEEE Ind. Elect. Soc., Nov. 2004, pp. 838–843.

[2] M. Molinas, J. A. Suul, and T. Undeland, "Low voltage ride through of wind farms with cage generators: STATCOM versus SVC,"IEEE Trans. Power Electron., vol. 23, no. 3, pp. 1104–1117, May 2008.

[3] Z. Chen, J. M. Guerrero, and F. Blaabjerg, "A review of the state of the art of power electronics for wind turbines,"IEEE Trans. Power Electron., vol. 24, no. 8, pp. 1859–1875, Aug. 2009.

[4] Y. Lei, A. Mullane, and G. Lightbody, "Modeling of the wind turbine with a doubly fed induction generator for grid integration studies,"IEEE Trans. Energy Convers., vol. 21, no. 1, pp. 257–264, Mar. 2006.

[5] R. Ganon, G. Sybille, and S. Bernard, "Modeling and real-time simulation of a doubly-fed induction generator driven by a wind turbine," presented at the Int. Conf. Power Systems Transients, Montreal, QC, Canada, Jun. 2005, Paper IPST05-162.

[6] H. Sun, Y. Ren, and H. Li, "DFIG wind power generation based on backto-back PWM converter," in Proc. IEEE Int. Conf. Mechatron. Autom., Aug. 2009, pp. 2276–2280.

[7] L. Xu and P. Cartwright, "Direct active and reactive power control of DFIG for wind energy generation,"IEEE Trans. Energy Convers., vol. 21, no. 3, pp. 750–758, Sep. 2006.

[8] S. Heier, Grid Integration of Wind Energy Conversion Systems. Hoboken, NJ, USA: Wiley, 2006.

[9] N. W. Miller, W. W. Price, and J. J. Sanchez-Gasca, "Dynamic modelling of GE 1.5 And 3.6 wind turbine-generators," GE Power Systems Energy Consulting, Gen. Elect. Int., Inc., Schenectady, NY, USA, Oct. 2003.

[10] R. Pena, J. C. Clare, and G. M. Asher, "Doubly fed induction generator using back-to-back PWM converters and its application to variable-speed wind-energy generation,"Proc. Inst. Elect. Eng.—Elect. Power Appl., vol. 143, no. 3, pp. 231–241, May 1996.

[11] Feijoo, J. Cidras, and C. Carrillo, "Third order model for the doubly-fed induction machine," Elect. Power Syst. Res., vol. 56, no. 2, pp. 121–127, Nov. 2000.

[12] T. Ghennam, E. M. Berkouk, and B. Francois, "DC-link voltage balancing algorithm using a space-vector hysteresis current control for three-level VSI applied for wind conversion system," inProc. Power Elect. Appl. Eur. Conf., Sep. 2007, pp. 1–10.

[13] M. Stiebler,Wind Energy Systems for Electric Power Generation. Berlin, Germany: Springer-Verlag, 2008